CHARACTERISATION OF A REFURBISHED 1½ STAGE TURBINE TEST RIG FOR FLOWFIELD MAPPING BEHIND BLADING WITH NON-AXISYMMETRIC CONTOURED ENDWALLS

Glen Snedden*, Thomas Roos*, Dwain Dunn* and David Gregory-Smith**

*CSIR, P O Box 395
Pretoria, 0001, South Africa
Tel: +2712 841-3094
Fax: +2712 349-1156
gsnedden@csir.co.za

**School of Engineering,
Durham University, South Road, Durham
DH1 3LE, UK
d.g.gregory-smith@durham.ac.uk

Abstract

This paper describes the results, to date, of collaboration between the CSIR (South Africa) and Durham University (UK). Furthermore the paper intends to demonstrate the capability and suitability of a refurbished 1½ stage turbine test rig to performing tests on blading featuring non-axisymmetric endwalls in a low-speed, rotating environment.

The test rig has been refurbished in such a way as to dramatically improve the measurement standards and to provide the highest degree of commonality with Durham University's equipment to ensure a common research thread. The characterisation of this turbine has revealed reduced power output levels when compared to the design data as a result of the tip vortex flows and an under-turning from the rotor as a result of the low Mach numbers. Although the results consistently yield lower power for the contoured rotor it is close to the experimental uncertainty.

In addition the use of rapidly prototyped blading has allowed for the manufacture of complex geometries at low cost, but with the addition of some new challenges.

Nomenclature

Symbol	
C_x	Axial velocity
N	Rotor wheel speed (RPM)
P_{00}	Inlet total pressure
P_2	Rotor exit static pressure
P_3	Turbine exit static pressure
P_R	Power
Q	Torque generated
V	Volume flow rate
Greek	
ΔP	Pressure drop
η	Efficiency
Subscripts	
Stage	Stage property
Turbine	1.5 stage turbine property

Introduction

Losses in a turbine can be attributed to three sources historically identified as: profile loss, endwall loss and leakage loss. The first refers to loss generated as a result of boundary layers on the blade where the flow can be described as two dimensional. The second is a combination of factors when studied in depth but is often referred to as loss resulting from secondary flows or three dimensional flows with in the blade passage. The last category refers to losses resulting from the flow over the tip of the blade, whether free tip or shrouded and the integration of that flow with the mainstream flow.

Denton (1993) states that only approximately ⅔ of the endwall loss can be attributed to entropy generation in the annulus boundary layers within, upstream and downstream of the blade row. A second component is attributed to the mixing loss of the inlet boundary layer amplified by the secondary flow. The third component is that of secondary kinetic energy which is of the order of ¼ of the total loss. Other contributions may arise from local flow separations, early transition and thickening of boundary layers as a result of the secondary flows.
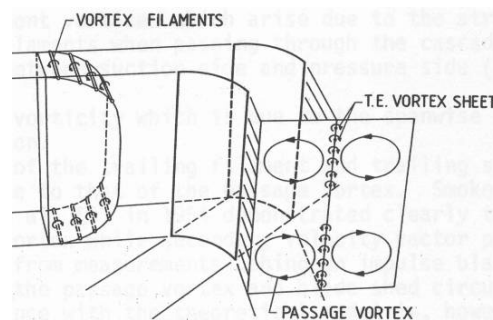

Figure 1: Classical model of secondary flow in a turbine passage (reproduced from Sieverding, 1985).
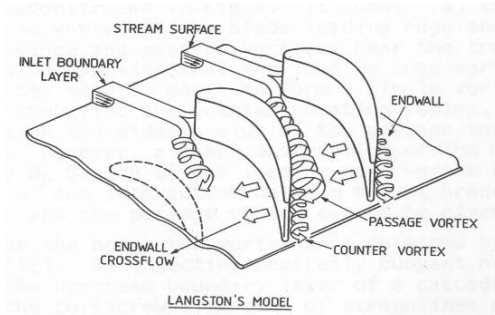
Figure 2: Langston's vortex models (reproduced from Sieverding (1985) who in turn reproduces them from the original author)
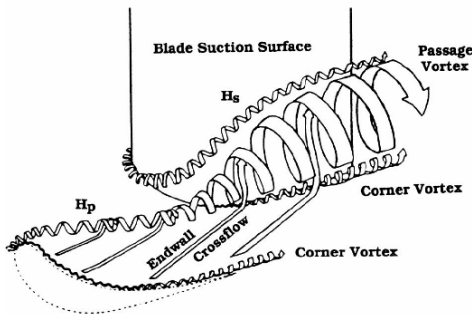

Figure 3: Vortex structure in a turbine cascade (reproduced from Moon, 2001)

To illustrate the complexity of the flows concerned, figures 1 to 3 illustrate the secondary flows from the classical model to what has been observed by different authors with techniques such as aerodynamic probes, laser sheet and smoke and laser Doppler anemometry.

Methods of limiting the generation of endwall loss

The following list is not exhaustive but summarises the types of techniques researched to reduce endwall losses or limit secondary flows and points to some of the researchers in each field of endeavour:

- Work distribution management and blade stacking variations such as the approach of Watanabe and Harada (1999).
- Blade lean and curve, currently the topic for research in the Durham cascade (Bagshaw et al, 2006).
- Leading edge bulbs and fillets (such as the work by Lethander et al, 2003 and Zess and Thole, 2002)
- Axisymmetric contouring has been investigated by many authors, for example Boyle et al (1981) who investigated the effects of radial

contractions which reduce surface velocities, thereby reducing the driving force for cross channel flows as well as reducing the radial driving forces for secondary flows, their experiments showed a 22% reduction in loss or a 0.8% increase in efficiency.

- Endwall fences, such as the work by Kawai (1994)
- Upstream tangential blowing, Bindon et al (1979)
- Air suction (Funazaki, 1996)
- Non-axisymmetric endwall contouring: in this department Gregory-Smith together with Rolls-Royce, Derby and Alstrom were first in presenting their findings, largely of CFD results and highly detailed measurements of the linear rotor cascade dubbed the 'Durham Cascade' which has in fact become an industry test case (Gregory-Smith, 1995). Brennan and Harvey et al (2001 & 2002) claim a 1/3rd reduction in endwall loss or a 0.59% increase in stage efficiency for the high pressure turbine, and even 0.9% efficiency improvement in the intermediate pressure turbine of the Rolls-Royce Trent 500 engine, using non-axisymmetric contouring.

The refurbished 1½ stage turbine test rig is intended to investigate this last method further, in a low speed, rotating environment.

The CSIR 1½ Stage Turbine Test Rig

A 1½ stage, low speed, turbine test rig, originally of the University of Natal (Morphis and Bindon, 1994) where it was used for tip loss measurements, has been installed and refurbished at the CSIR in Pretoria. Figures 4 and 5 indicate the general layout and instrumentation of the test rig. The design speed of the rig is 3000RPM, and the radial fan drawing atmospheric air through the rig induces a pressure drop of 4.8kPa for a massflow of 3.39kg/s, corresponding to an inlet velocity of about 25m/s. The radial fan is driven by a 30kW electric motor with variable speed control, and the turbine power is absorbed by a hydraulic motor, giving independent rotor speed control. The tables, which follow, describe the instrumentation and its associated accuracies, as well as the control stability and uncertainty.

Control and data acquisition is achieved through a Siemens S7-200 PLC

12 bit A/D with Wincc Flexible Scada software.

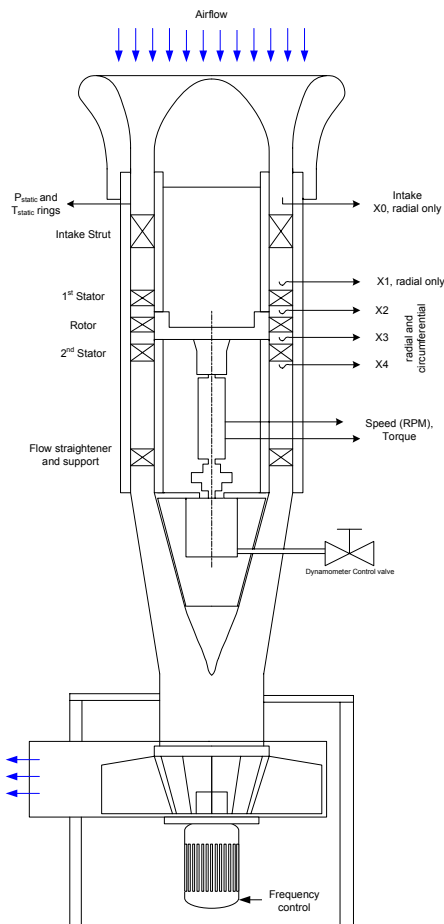Figure 4: The refurbished test stand at the CSIR

Figure 5: Schematic of 1½ stage turbine and control and measurement instrumentation

Blading Design and Manufacturing

The blading was designed utilising the inverse design method (NREC, 1972) and the requirement to utilise the Durham cascade profile at the Rotor hub in order to utilise the P2 endwall profile shown in figure 7. The initial idea was to have a repeating stator design but as the constraints imposed by the test rig capabilities and the rotor hub design resulted in a highly twisted rotor blade it was abandoned in favour of a design with non-axial rotor outlet, reducing blade twist. This finally resulted in a 1½ stage design in which the Durham cascade profile could be repeated on the hub of both the rotor and 2nd stator. This gives the advantage of allowing the examination of the application of non-axisymmetric endwalls of Ingram (2003) in a rotating and annular environment as well as stationary with upstream unsteadiness. The final design is given in Appendix A and summarised below in table 2 and figure 6. The thin stator tip profile (about 1mm) is a result of attempting to limit axial chord to prevent probe/blade interference in the measurement plane.

Table 1: Instrumentation

| Primary Instrumentation		
Parameter	**Instrument**	**Uncertainty**
Torque	Himmelstein MCRT	±0.03N.m
Speed	28002T(5-2)CNA-G + Model 721 Mechanical Power Instrument	2RPM
Barometric Pressure	Siemens Sitrans P 7MF4233-1FA10-1AB6-Z A02+B11	0.05% of full scale
Differential Pressure	5 x Siemens Sitrans P 7MF4433-1CA02-1AB6-Z A02+B11	0.05% of full scale
Temperature	PT1000 RTD's	±0.05°C
Secondary Instrumentation		
Steady Flow mapping	Aeroprobe CPC5-C159-305-015.3-16 5 hole cobra probe (1.59mm Ø head)	0.8% in Velocity magnitude, 0.4° in flow angles
Turbulence	TSI 1211-20 single component film	±0.77% mean velocity*
Unsteady Flow mapping	TSI 1240-20 / 1247A-10 X-probe (film)	±0.77% mean velocity, ±6% of variance*
Tangential Traverse	Custom cable system rotating the outer casing	Better than 0.01°
Radial and Yaw traverse	Rotodata Mini actuator	0.01mm 0.1°

* Stamatios (2002)
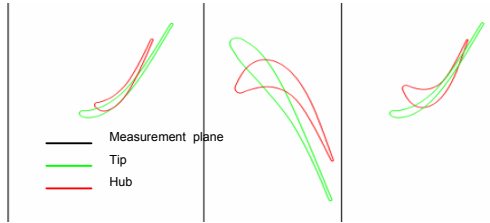
Figure 6: 1½ Stage turbine design

The P2 endwall design was chosen as it was both the most successful of the Durham endwall designs and the most practical as it limits the profiling to the blade passage without upstream or downstream extensions to interfere with the respective stators.

The endwall design was reverse-engineered from the available literature, (Ingram (2003)) and the knowledge of the design system and approach as outlined by Harvey et al (2000).

Table 2: Design summary

Inlet		
Axial Velocity		21.38 m/s
Rotational Speed		2300 RPM
1st Stator		
No. of Blades		30
Inlet Angle	Hub	0°
	Casing	0°
Outlet Angle	Hub	68.26°
	Casing	61.20°
Rotor		
No. of Blades		20
Inlet Angle	Hub	42.75°
	Casing	-23.98°
Outlet Angle	Hub	-68.00°
	Casing	-71.15°
Stage Power		3.87 kW
Stage Pressure Ratio		1.0393
2nd Stator		
No. of Blades		30
Inlet Angle	Hub	42.75°
	Casing	35.45°
Outlet Angle	Hub	68.00°
	Casing	61.77°

Finally the choice of manufacturing technique was rapid prototyping in this case utilising a laser sintering technique available at the Central University of Technology in Bloemfontein, South Africa. The material is Fine Polyamide PA2200 as used on the EOSINT P system. This material was a late selection resulting from the failure of the rapid prototyping machine using a Renshape SL7580 epoxy and offered equivalent strength to weight ratio, but a reduced flexural modulus. Figure 8 shows the completed blading, showing two blades each for the rotor and 2nd stage stator, the annular hub on the left and non-

axisymmetric contoured hub on the right. The rapid prototyping material has proven highly capable in producing the complex shape of the endwall features quickly and cheaply.
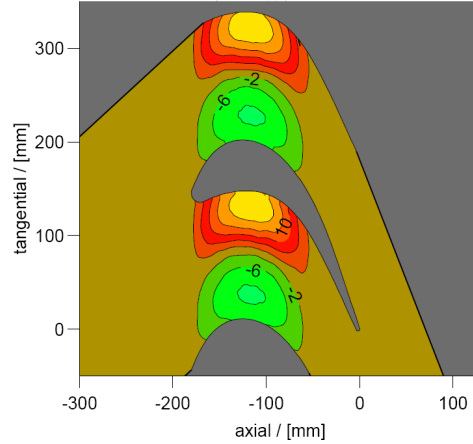
Contour interval 4mm

Figure 7: The Durham P2 contoured endwall as reported by Ingram (2003)
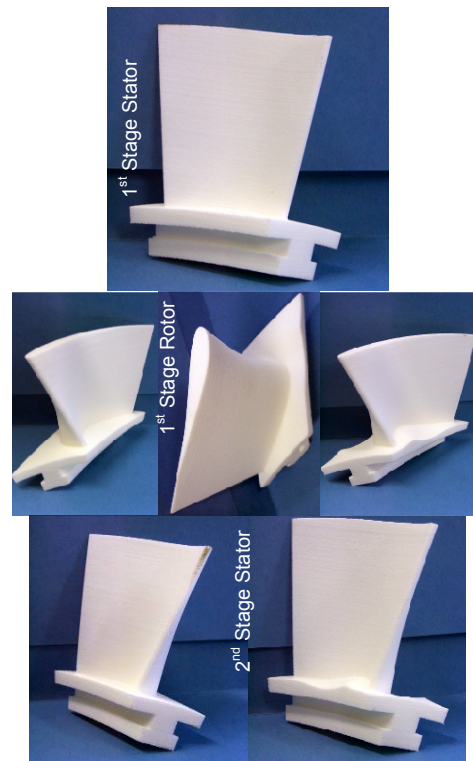

Figure 8: Final blading as sintered.

Turbine Characterisation results

Inlet turbulence intensity was measured utilising the single hot-film probe and TSI's Thermal Pro software and found to be less than 1%. Table 3 gives

the results for two different inlet access points.

Table 3: Inlet turbulence

Intake	
Maximum	0.71%
Mean	0.6364%
Minimum	0.58%
X0 Traverse Position	
Maximum	0.94%
Mean	0.7438%
Minimum	0.634%

The turbine was characterised utilising the torque and speed transducers and single static pressure ports after the rotor (X2 traverse position (see figure 4) and after the complete 1½ stage turbine (X3 traverse position). The method was a modified version of the British Standard BS848 as follows:

$$\Delta P_{stage} = P_{00} - P_2$$

$$\Delta P_{turbine} = P_{00} - P_3$$

$$P_R = \frac{2\pi}{60} QN$$

$$\eta = \frac{\Delta P \cdot V}{P_R}$$

Figures 9 and 10 indicate that the actual turbine power output and efficiency is significantly below that predicted using the TPERF meanline, off-design code (NREC, 1972) during design. Disc windage using the correlations of Daily and Nece (1960) combined with bearing loss accounts for only some 12W which does not explain this disparity.
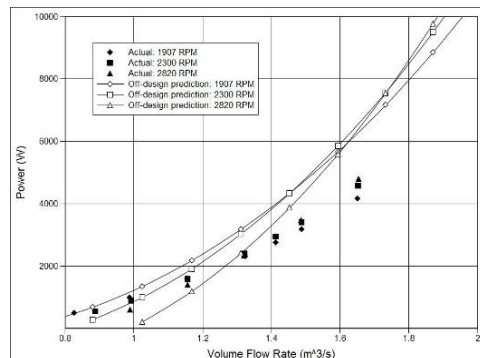

Figure 9: Comparison of predictions and experimental turbine output power versus volume flow rate
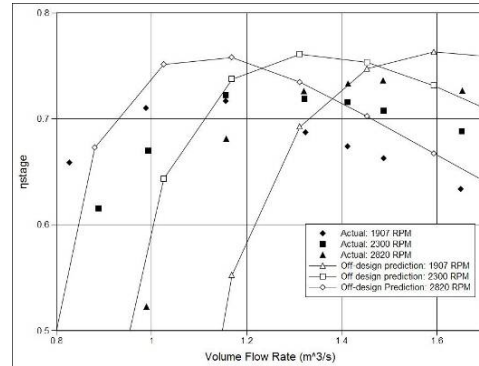

Figure 10: Comparison of predicted and experimental turbine stage efficiency versus volume flow rate

Two techniques for varying the stage flow factor were experimented with; the first was to fix the turbine wheel speed and varying the volume flow rate through the machine. The wheel speeds were selected such that they should provide for a 5° rotor blade incidence change either side of the design point at the hub.

Figures 11 to 13 give the results of this first series of tests. Once again the power output is below the design point by some 24% and the stage efficiency appears to be only 1% below the prediction, as a result of the stage pressure drop being reduced in similar proportion to the power compared to the design predictions. The efficiency of the 1½ stage system is similarly well predicted.

The second technique of these results is the comparison of the annular and contoured turbines. There is little to chose between the designs in terms of the power output (figure 11), or the stage efficiency (figure 12). In addition Figure 12 includes error bars indicating the uncertainty in the results which indicate that although the contoured endwall turbine results are consistently lower powered and less efficient, they are within experimental uncertainty. The turbine efficiency results, figure 13, however, indicate a greater difference between the turbines; the contoured turbine is consistently 1 to 2% less efficient than the annular endwall design. This latter result suggests that the flow into the 2nd stator has higher secondary loss or more variable outlet flow angle than that of the annular turbine.
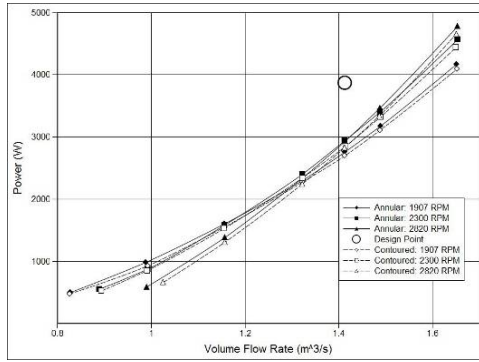
Figure 11: Constant speed lines, power versus volume flow rate.
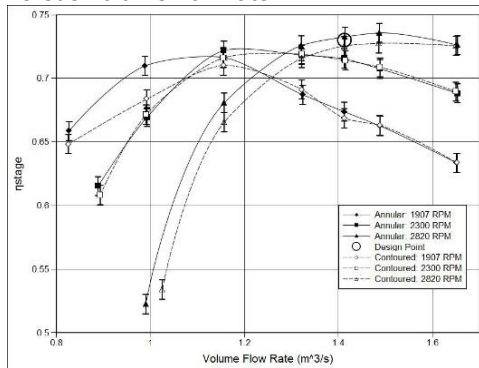
Figure 12: Constant speed lines, stage efficiency versus volume flow rate
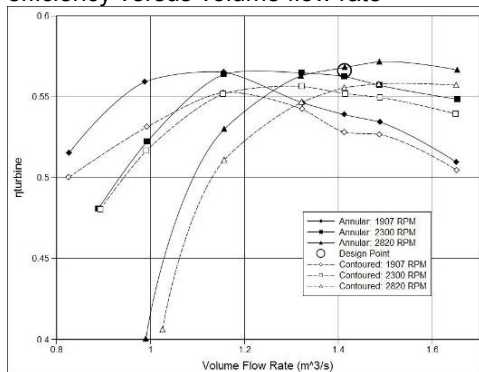
Figure 13: Constant speed lines, turbine efficiency versus volume flow rate
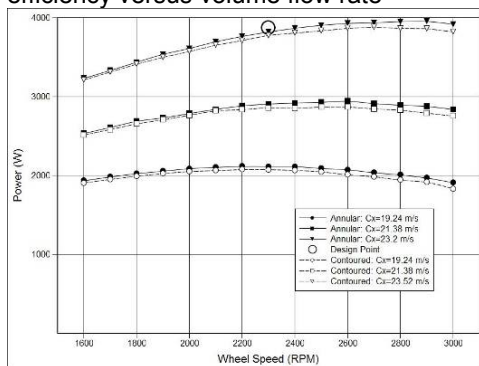
Figure 14: Constant flow rate lines, power versus wheel speed
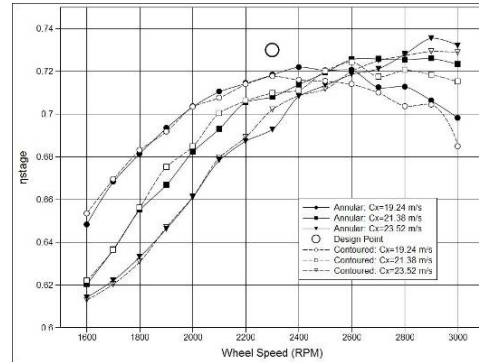
Figure 15: Constant flow rate lines, stage efficiency versus wheel speed
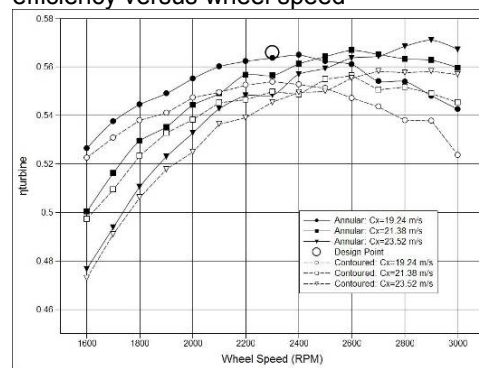
Figure 16: Constant flow rate lines, turbine efficiency versus wheel speed

The second control technique used was to control the flow rate and vary the wheel speed, in this case the flow rates were adjusted by 10% either side of the design flow rate, these results are captured in figures 14 to 16.

Once again the results indicate similar disparities between design and actual results as well as between annular and contoured turbine designs as the first technique.

Finally all the results are collated into two further figures, 17 and 18 and plotted in non-dimensional quantities of stage load and flow factors, after the method of the National Gas Turbine Establishment as followed by Saravanamuttoo et al. (2001). Once again the conclusions are consistent with previous results, but the repeatability between tests is shown to be very good.

After a visual check for untwist or flutter in the stators, the turning of the rotor was scrutinised. Figure 18, with its unmistakably linear characteristic suggested that with changing incidence there is no change in rotor outlet angle as a result of the elimination of a separation effect, as this would have resulted in a curved characteristic. Figures 19 and 20
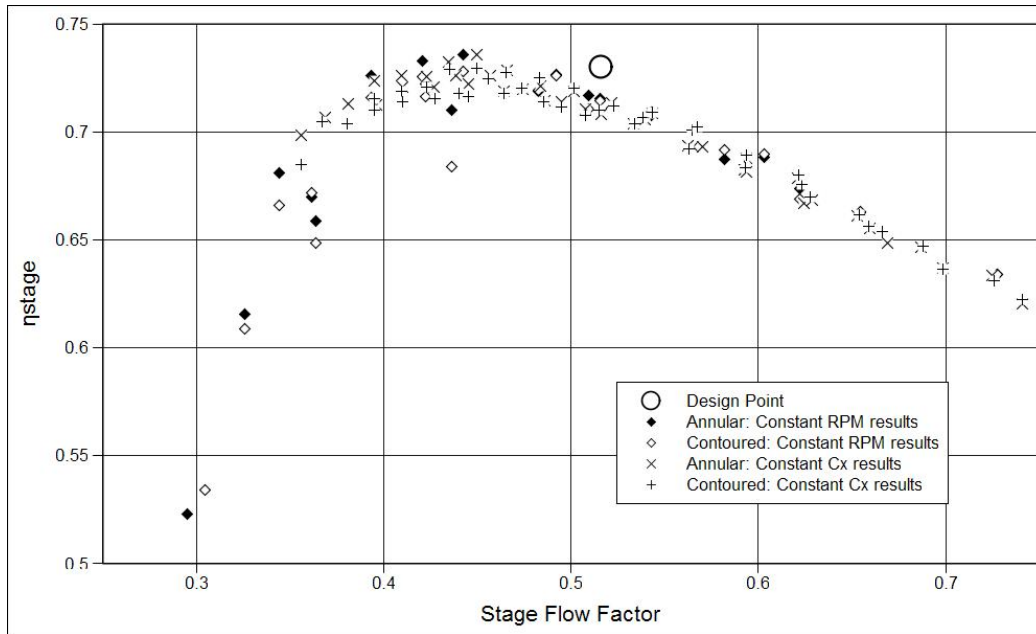
Figure 17: Stage efficiency versus stage flow factor
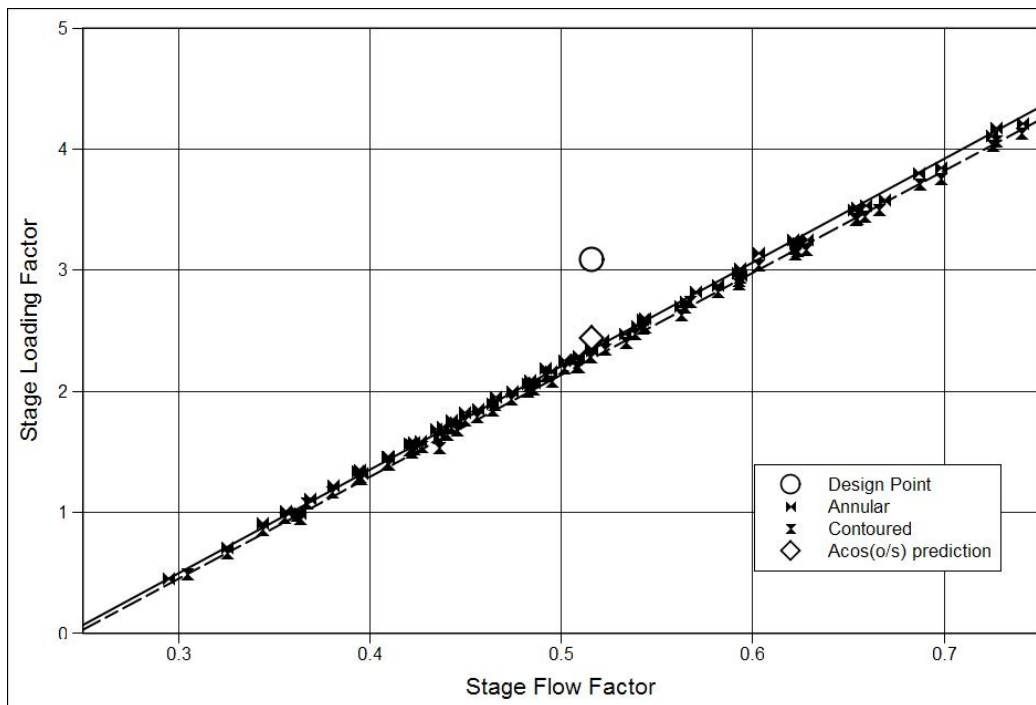
Figure 18: Stage loading factor versus stage flow factor

were then created by performing crude null-yawing traverses behind the stator at roughly mid-chord, as well as behind the rotor. The discrepancies between design and experiment seen on the stator were confirmed by a visual inspection of the 1st stage stators, which are bowed in a manner in parallel with figure 19, even to the point of having small cracks at the inflexion point seen in figure 19 at a span of 42mm.

The results after the rotor (figure 20) indicate the source of the reduced power, under-turning by the rotor. Although NREC (1972) utilises the cosine rule to determine outlet flow angle, the design code takes no account for the reduction in flow angles at low Mach numbers, in accordance with Saravanamuttoo (2001).
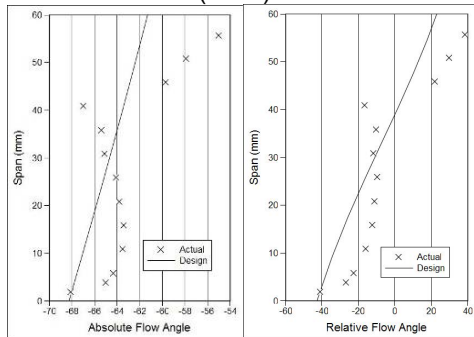
Figure 19: 1st Stator outlet angle (contoured turbine)
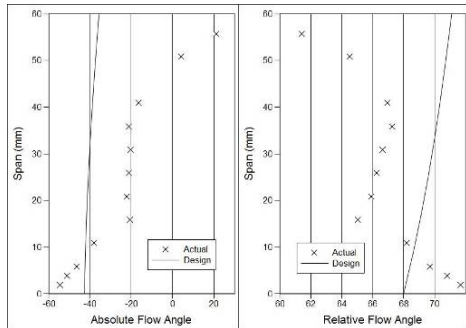
Figure 20: Rotor outlet flow angle (contoured turbine)

The implication of the under-turning is indicated on Figure 18 (annotated as 'Acos(o/s) prediction') and agrees well with the experimental results. Apart from reduced rotor power the implication of the under-turning is that an adjustment to the rotor speed will have to be made to provide flow angles closer to the design point for any tests on the 2nd Stator.

Conclusions

The 1½ stage turbine test rig has been fully refurbished and is now available for performing tests on any variety of turbine geometries and features. The first such turbine design has been extensively characterised. The near future will see a detailed mapping of steady and unsteady flow features upstream and downstream of each blade row.

The rapid prototyping material has proven highly capable both in producing the complex shape of features such as the endwall contours, and in terms of having sufficient strength to withstand the rotation forces in the rotor. In fact the material has remarkable resilience and can easily be repaired using cyanoacrylate gel. The flexural modulus of the material is however low and has led to significant bowing of the trailing edge of the 1st stator. This, in combination with an expansive tip loss vortex (a combination of relatively large tip gaps, and on all blade rows, rather than the traditional hub gaps or shrouded stators), and underturning in the rotor has led to a large reduction in the stage loading factor. A future stator ring will have to take account of the low flexural modulus of the sintered polymide material and feature increased blade thickness in the midchord region tapering towards the trailing edge, leading to a longer blade chord. Little comment can be made about the differences between the contoured and annular endwalls as the differences measured are close to experimental uncertainty.

References

1. Bagshaw DA, Gregory-Smith D, Ingram G, and Stakes MR, "A turbine cascade facility for secondary flow research," *ASME Turbo Expo 2006: Power for Land Sea and Air*, ASME GT2006-90868, 2006.
2. Bindon JP, Aburwin BA, and MacCallum NRL, "Comparison of transverse injection effects in annular and in straight turbine cascades," ASME 79-GT-17, 1979.
3. Boyle RJ, Rholik HE, and Goldman LJ, "Analytic investigation of effect of end-wall contouring on stator performance," NASA-TP-1943, E-719, 1981.
4. Brennan G, Harvey N, Rose MG, Fomison N, and Taylor MD, "Improving the efficiency of the Trent

500 HP turbine using non-axisymmetric end walls: Part 1 Turbine design," *ASME TURBO EXPO 2001*, ASME 2001-GT-0444, 2001.

5. British Standard BS848

6. Daily JW and Nece RE, "Chamber dimension effects on induced flow and friction resistance of enclosed rotating disks," Transactions of ASME Journal of Basic Engineering, pp. 217-232, March 1990.

7. Denton JD, "Loss mechanisms in turbomachines," *ASME Gas Turbine Congress*, Scholars Paper, 1993.

8. Funazaki K, Endo T, and Tanuma T, "Reduction of secondary flow effects in a linear cascade by use of an air suction from the endwall," ASME 96-TA-51, 1996.

9. Gregory-Smith D, "3D flow simulation in turbomachinery - The ERCOFTAC Seminar and Workshop II, January 1994," VDI Berichte, No. 1185, 1995, pp. 35-49.

10. Harvey N, Brennan G, Newman DA, and Rose MG, "Improving turbine efficiency using non-axisymmetric endwalls: Validation in the multi-row environment and with low aspect ratio blading," *ASME TURBO EXPO 2002*, ASME 2002-GT-30337, 2002.

11. Ingram G. Endwall profiling for the reduction of secondary flow in turbines. 2003. Durham University, UK.

12. Kawai T, "Effect of combined boundary layer fences on turbine secondary flow and losses," *JSME International Journal, Series B: Fluids and Thermal Engineering*, Vol. 37, No. 2, 1994, pp. 377-384.

13. Langston LS, Nice ML, and Hooper RM, "Three-dimensional flow within a turbine cascade passage," *Transactions of ASME, Journal of Engineering for Power*, 1977, pp. 21-28.

14. Moon YJ and Sung-Ryon K, "Counter-rotating streamwise vortex formation in the turbine cascade with endwall fence," *Computers & Fluids*, Vol. 30, No. No. 4, 2001, pp. 473-490.

15. Morphis G and Bindon JP, "The performance of a low speed one and a half stage axial turbine with varying rotor tip clearance and tip gap geometry," *International Gas Turbine and Aeroengine Congress and Exposition*, ASME 94-GT-481, 1994.

16. NREC, "The design and performance analysis of axial-flow turbines: Volumes I and II," Northern Research and Engineering Corporation, 1972

17. Saravanamuttoo HIH, Rogers CFC and Cohen H, "Gas turbine theory," 5th Edition, Prentice Hall, 2001.

18. Sieverding CH, "Recent progress in the understanding of the basic aspects of secondary flows in turbine blade passages," *Transactions of ASME, Journal of Engineering for Gas Turbines and Power*, Vol. 107, 1985, pp. 248-252.

19. Stamatios P "Control of particles and turbulence using a piezoelectric actuator," PhD Thesis, University of Minnesota, 2002.

20. Watanabe H and Harada H, "Supression of secondary flows in turbine nozzle with controlled stacking shape and exit circulation by 3D inverse design method," ASME 99-GT-72, 1999.

21. Zess GA and Thole KA, "Computational design and experimental evaluation of using a leading edge fillet on a gas turbine vane," *Transactions of ASME, Journal of Turbomachinery*, Vol. 124, 2002, pp. 167-175.

Appendix A: Turbine Geometry

1st Stator Hub

Pressure Surface

X	Y	Z
141.8	7.5	-79.6
141.8	7.2	-79.5
141.8	7.0	-79.4
141.8	6.8	-79.2
141.8	6.7	-79.0
141.8	6.6	-78.8
141.8	6.6	-78.5
141.9	6.5	-78.2
141.9	6.0	-76.2
141.9	5.3	-74.3
141.9	4.3	-72.5
142.0	3.0	-70.9
142.0	1.7	-69.4
142.0	0.2	-67.9
142.0	-1.3	-66.6
142.0	-3.0	-65.4
141.9	-4.7	-64.3
141.9	-6.5	-63.3
141.8	-8.3	-62.3
141.6	-10.1	-61.4
141.5	-12.0	-60.4
141.3	-13.8	-59.5
141.1	-15.6	-58.7
140.9	-17.5	-57.8
140.7	-19.4	-57.0
140.4	-21.2	-56.2
140.2	-22.8	-55.5
140.1	-22.9	-55.4
140.1	-23.0	-55.3
140.1	-23.0	-55.2
140.1	-23.0	-55.1
140.1	-23.0	-54.9
140.1	-23.0	-54.8

Suction Surface

X	Y	Z
141.8	7.5	-79.6
141.8	7.7	-79.6
141.8	8.0	-79.6
141.8	8.2	-79.6
141.7	8.5	-79.4
141.7	8.7	-79.3
141.7	9.0	-79.0
141.6	10.3	-77.0
141.6	10.5	-74.7
141.7	9.7	-72.5
141.8	8.3	-70.6
141.8	6.7	-68.9
141.9	4.9	-67.4
142.0	2.9	-66.1
142.0	0.9	-64.9
142.0	-1.2	-63.7
142.0	-3.3	-62.7
141.9	-5.4	-61.7
141.8	-7.5	-60.7
141.7	-9.7	-59.8
141.5	-11.8	-58.8
141.3	-14.0	-58.0
141.1	-16.2	-57.1
140.8	-18.4	-56.2
140.5	-20.5	-55.3
140.2	-22.4	-54.6
140.2	-22.5	-54.6
140.2	-22.6	-54.6
140.2	-22.8	-54.6
140.1	-22.9	-54.7
140.1	-23.0	-54.8

1st Stator Tip

Pressure Surface

X	Y	Z
202.2	11.3	-86.1
202.2	11.0	-86.0
202.2	10.8	-85.8
202.2	10.6	-85.6
202.2	10.5	-85.3
202.2	10.4	-85.1
202.2	10.4	-84.8
202.2	10.5	-83.7
202.3	10.0	-80.7
202.3	9.1	-77.9
202.3	7.8	-75.2
202.4	6.2	-72.6
202.5	4.4	-70.2
202.5	2.3	-68.0
202.5	0.1	-66.0
202.5	-2.3	-64.1
202.4	-4.7	-62.3
202.4	-7.2	-60.5
202.3	-9.7	-58.9
202.1	-12.3	-57.3
202.0	-14.8	-55.7
201.7	-17.4	-54.2
201.5	-20.0	-52.7
201.2	-22.7	-51.2
200.9	-25.3	-49.7
200.6	-27.9	-48.3
200.2	-30.1	-47.0
200.2	-30.3	-46.9
200.2	-30.3	-46.8
200.2	-30.4	-46.7
200.2	-30.4	-46.5
200.2	-30.4	-46.4

Suction Surface

X	Y	Z
202.2	11.3	-86.1
202.2	11.5	-86.1
202.2	11.8	-86.1
202.1	12.1	-86.1
202.1	12.3	-86.0
202.1	12.5	-85.8
202.1	13.2	-85.0
202.0	13.7	-81.8
202.1	13.1	-78.6
202.2	11.8	-75.7
202.3	10.0	-72.9
202.3	8.0	-70.4
202.4	5.7	-68.1
202.5	3.2	-66.0
202.5	0.6	-64.0
202.5	-2.0	-62.1
202.4	-4.7	-60.3
202.4	-7.5	-58.6
202.2	-10.2	-56.9
202.1	-13.0	-55.3
201.9	-15.9	-53.7
201.6	-18.7	-52.1
201.4	-21.5	-50.6
201.0	-24.4	-49.0
200.7	-27.2	-47.5
200.3	-29.6	-46.1
200.3	-29.8	-46.1
200.3	-29.9	-46.0
200.3	-30.0	-46.1
200.2	-30.2	-46.1
200.2	-30.3	-46.2
200.2	-30.4	-46.4

Rotor Hub

Pressure Surface

X	Y	Z
142.0	1.4	-18.8
142.0	0.0	-19.3
142.0	-1.6	-18.9
142.0	-3.0	-18.3
141.9	-4.5	-17.6
141.9	-5.9	-16.9
141.8	-7.3	-16.1
141.7	-8.6	-15.2
141.7	-9.8	-14.1
141.6	-10.9	-13.0
141.5	-11.8	-11.7
141.4	-12.6	-10.3
141.4	-13.1	-8.7
141.4	-13.3	-7.2
141.4	-13.3	-5.6
141.4	-13.1	-4.0
141.4	-12.6	-2.4
141.5	-12.0	-1.0
141.6	-11.2	0.4
141.6	-10.3	1.7
141.7	-9.3	3.0
141.8	-8.2	4.1
141.8	-7.0	5.2
141.9	-5.8	6.2
141.9	-4.5	7.2
142.0	-3.2	8.1
142.0	-1.9	9.0
142.0	-0.5	9.8
142.0	0.9	10.6
142.0	2.3	11.3
142.0	3.8	12.1
141.9	5.2	12.7
141.8	6.7	13.4
141.8	8.1	14.0
141.7	9.6	14.6
141.6	11.1	15.2
141.4	12.6	15.8
141.3	14.1	16.3
141.1	15.6	16.9
141.0	17.1	17.4
140.8	18.6	17.9
140.6	20.1	18.4
140.3	21.6	18.9
140.1	23.1	19.4
139.9	24.6	19.9
139.6	26.1	20.4
139.3	27.6	20.9
139.0	29.1	21.4
138.7	30.6	21.9
138.3	32.1	22.4
138.0	33.5	22.9
137.9	34.0	22.7

Suction Surface

X	Y	Z
142.0	1.4	-18.8
142.0	2.1	-17.7
142.0	2.1	-16.5
142.0	1.7	-15.4
142.0	1.2	-14.3
142.0	0.7	-13.1
142.0	0.3	-12.0
142.0	0.0	-10.8
142.0	-0.3	-9.6
142.0	-0.5	-8.4
142.0	-0.6	-7.2
142.0	-0.7	-6.0
142.0	-0.7	-4.8
142.0	-0.6	-3.5
142.0	-0.4	-2.3
142.0	-0.1	-1.2
142.0	0.3	0.0
142.0	0.8	1.1
142.0	1.4	2.2
142.0	2.0	3.2
142.0	2.7	4.2
142.0	3.5	5.2
141.9	4.4	6.0
141.9	5.3	6.9
141.9	6.2	7.6
141.8	7.2	8.4
141.8	8.2	9.1
141.7	9.2	9.7
141.6	10.3	10.4
141.5	11.3	11.0
141.5	12.4	11.6
141.4	13.4	12.2
141.3	14.5	12.8
141.1	15.6	13.4
141.0	16.6	13.9
140.9	17.7	14.5
140.7	18.8	15.0
140.6	19.9	15.5
140.4	21.0	16.1
140.3	22.1	16.6
140.1	23.2	17.1
139.9	24.3	17.6
139.7	25.4	18.2
139.5	26.4	18.7
139.3	27.5	19.2
139.1	28.6	19.7
138.9	29.7	20.2
138.6	30.8	20.7
138.4	31.9	21.2
138.1	33.0	21.7
137.9	34.0	22.3
137.9	34.0	22.7

Rotor Tip

Pressure Surface

X	Y	Z
200.8	-22.0	-21.4
200.8	-22.0	-21.4
200.8	-21.8	-21.5
200.8	-21.5	-21.5
200.9	-21.3	-21.6
200.9	-21.1	-21.6
200.9	-20.9	-21.6
200.9	-20.7	-21.6
201.0	-20.4	-21.5
201.0	-20.2	-21.5
201.3	-17.0	-19.8
201.6	-13.4	-17.7
201.7	-10.1	-15.1
201.9	-7.0	-12.5
202.0	-3.8	-9.8
202.0	-0.7	-7.2
202.0	2.5	-4.6
201.9	5.8	-2.1
201.8	9.1	0.4
201.6	12.4	2.7
201.4	15.9	4.9
201.1	19.5	6.9
200.7	23.1	8.8
200.2	26.8	10.6
199.7	30.5	12.3
199.1	34.2	14.0
198.4	37.9	15.6
197.7	41.7	17.1
196.8	45.4	18.5
195.9	49.2	19.9
195.1	52.2	21.1
195.1	52.3	21.2
195.1	52.4	21.2
195.1	52.4	21.3
195.1	52.5	21.3
195.1	52.5	21.4
195.0	52.5	21.4
195.0	52.6	21.5
195.0	52.6	21.6
195.0	52.6	21.6
195.0	52.6	21.7
195.0	52.6	21.8
195.0	52.6	21.9
195.0	52.6	21.9

Suction Surface

X	Y	Z
200.8	-22.0	-21.4
200.8	-22.2	-21.3
200.8	-22.3	-21.2
200.7	-22.5	-21.1
200.7	-22.7	-20.9
200.7	-22.8	-20.7
200.7	-23.0	-20.6
200.7	-23.1	-20.4
200.6	-23.5	-18.7
200.8	-21.8	-14.4
201.1	-18.9	-10.7
201.4	-15.5	-7.6
201.7	-11.6	-4.8
201.9	-7.6	-2.4
202.0	-3.5	-0.2
202.0	0.7	1.8
201.9	5.0	3.8
201.8	9.3	5.6
201.5	13.6	7.4
201.2	18.0	9.2
200.8	22.3	10.9
200.2	26.6	12.6
199.6	31.0	14.3
198.9	35.3	16.0
198.1	39.6	17.6
197.2	43.9	19.2
196.2	48.2	20.8
195.2	51.8	22.2
195.2	51.9	22.3
195.2	52.0	22.3
195.2	52.0	22.3
195.2	52.1	22.3
195.1	52.2	22.3
195.1	52.2	22.2
195.1	52.3	22.2
195.1	52.4	22.2
195.1	52.4	22.1
195.1	52.5	22.1
195.1	52.5	22.0
195.0	52.5	21.9
195.0	52.6	21.9

2nd Stator Hub
Identical to rotor hub, mirrored and scaled to an axial chord of 28.16 mm

2nd Stator Tip

Pressure Surface

X	Y	Z
202.2	11.2	47.3
202.2	11.1	47.4
202.2	10.9	47.5
202.2	10.7	47.6
202.2	10.6	47.8
202.2	10.5	48.0
202.2	10.5	48.2
202.2	10.4	48.4
202.2	10.4	48.6
202.2	10.5	49.6
202.3	10.0	52.6
202.3	9.1	55.5
202.3	7.8	58.2
202.4	6.2	60.8
202.5	4.4	63.1
202.5	2.3	65.4
202.5	0.1	67.4
202.5	-2.3	69.3
202.4	-4.7	71.1
202.4	-7.2	72.8
202.3	-9.7	74.5
202.1	-12.3	76.1
202.0	-14.8	77.7
201.7	-17.4	79.2
201.5	-20.0	80.7
201.2	-22.7	82.2
200.9	-25.3	83.6
200.6	-27.9	85.1
200.2	-30.4	86.5
200.2	-30.5	86.6
200.2	-30.6	86.6
200.2	-30.6	86.7
200.2	-30.7	86.8
200.2	-30.7	87.0
200.2	-30.7	87.1
200.2	-30.6	87.2
200.2	-30.6	87.3

Suction Surface

X	Y	Z
202.2	11.2	47.3
202.2	11.4	47.2
202.2	11.6	47.2
202.2	11.8	47.2
202.1	12.0	47.3
202.1	12.2	47.3
202.1	12.4	47.4
202.1	12.5	47.6
202.1	13.2	48.4
202.0	13.7	51.6
202.1	13.1	54.7
202.2	11.8	57.7
202.3	10.0	60.4
202.3	8.0	62.9
202.4	5.7	65.2
202.5	3.2	67.4
202.5	0.6	69.3
202.5	-2.0	71.2
202.4	-4.7	73.0
202.4	-7.5	74.8
202.2	-10.2	76.4
202.1	-13.0	78.1
201.9	-15.9	79.7
201.6	-18.7	81.2
201.4	-21.5	82.8
201.0	-24.4	84.3
200.7	-27.2	85.9
200.3	-29.9	87.4
200.3	-30.0	87.4
200.2	-30.1	87.5
200.2	-30.2	87.5
200.2	-30.3	87.4
200.2	-30.4	87.4
200.2	-30.5	87.3
200.2	-30.6	87.3